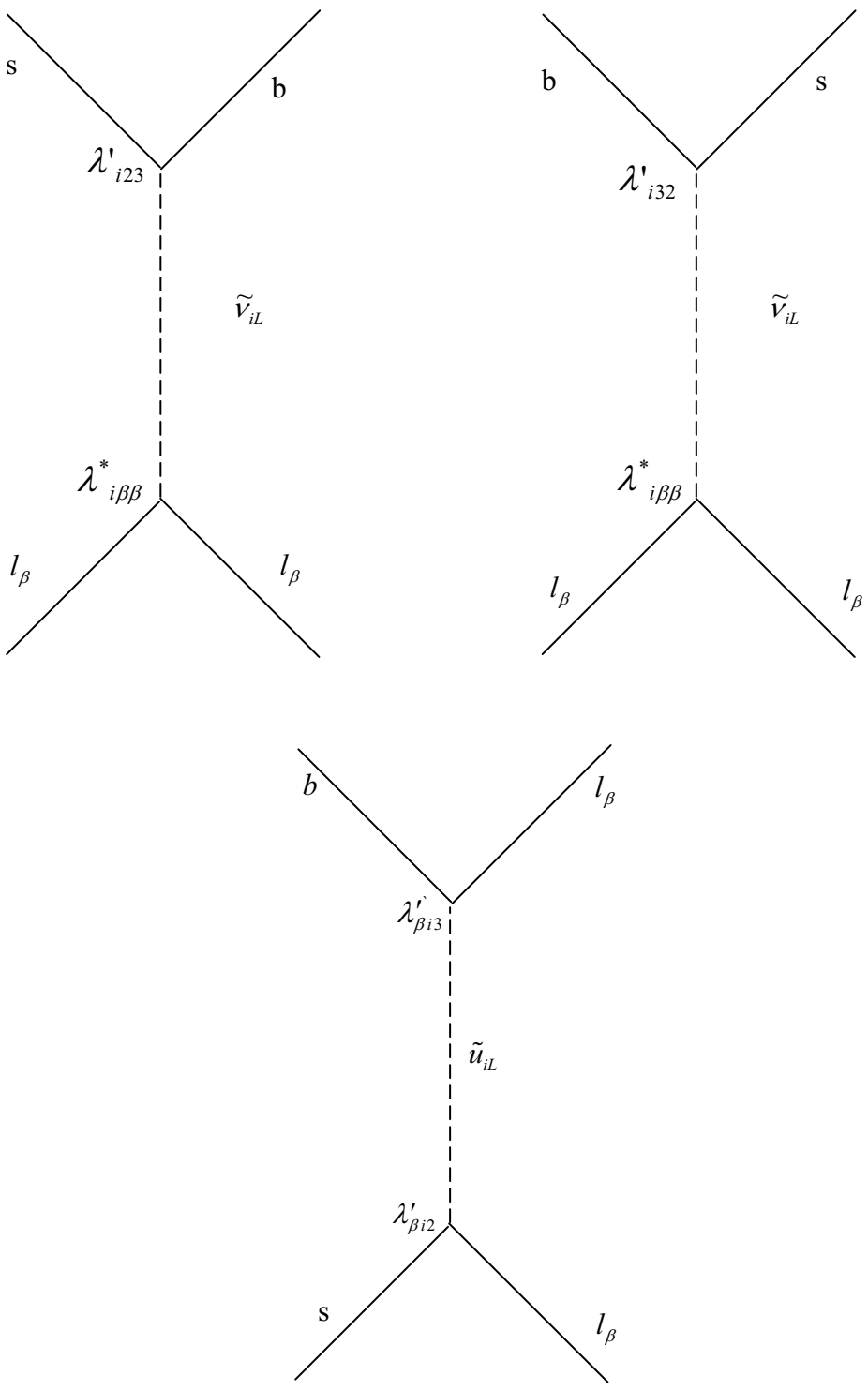

Fig. 1 Tree-Level diagrams contributing to charged meson decays $B^+ \to K^+ l_\beta^+ l_\beta^- (b \to s l_\beta^+ l_\beta^-)$.

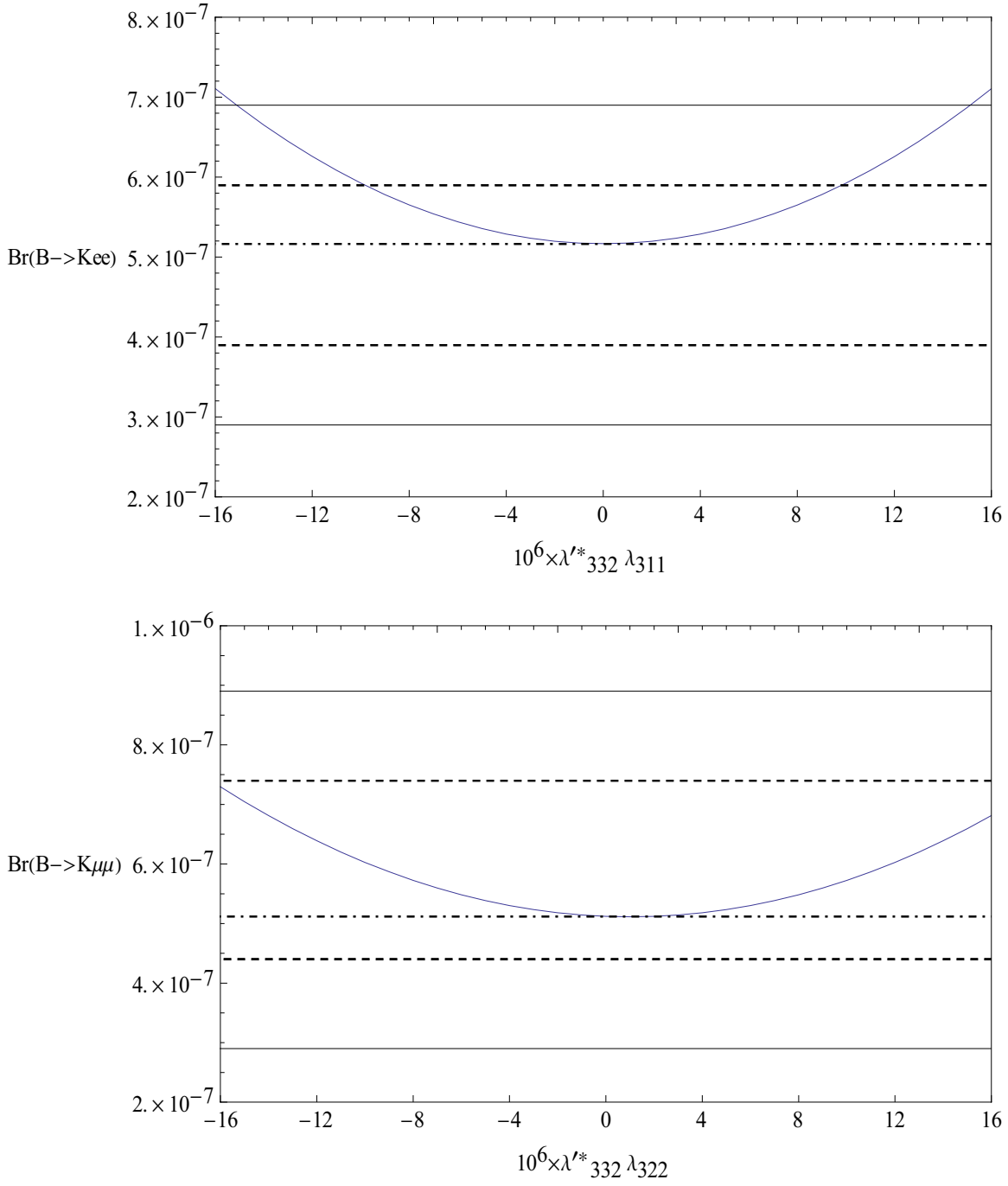

Fig 2. Dependence of total branching fraction with real R-parity Yukawa couplings within 1σ (dashed) and 2 σ (solid) level in observed value of branching fraction. SM prediction is given by Dotted dash line). Single coupling dominance has been assumed. $\lambda'_{332}\,\lambda_{3\alpha a}$ (α=1, 2) is expressed in the units of $(\frac{m_{\tilde{\nu}_L}}{100\,GeV})^2$.

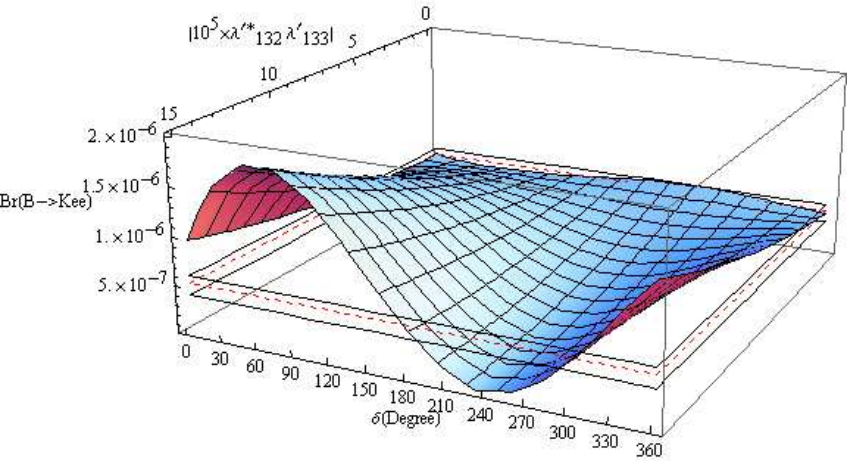

(a)

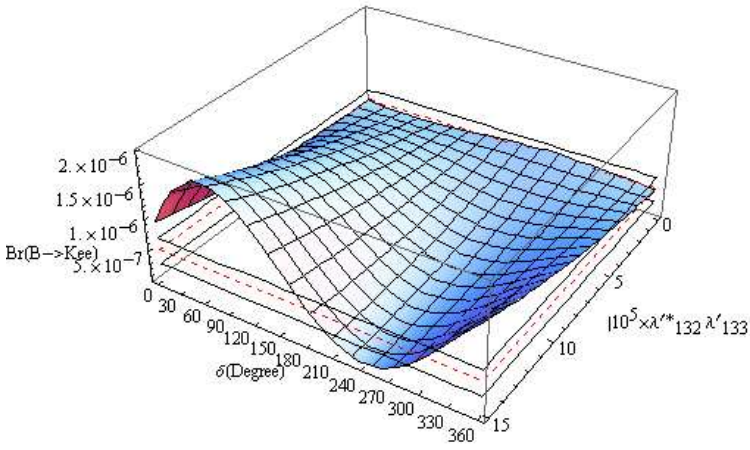

(b)

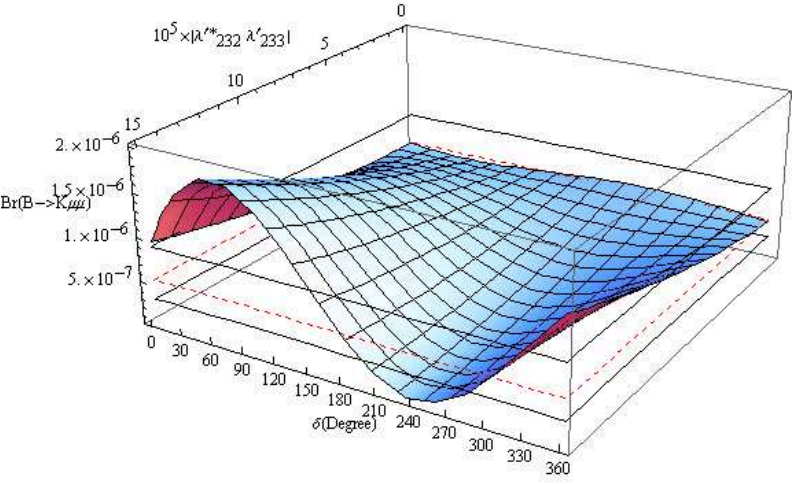

(c)

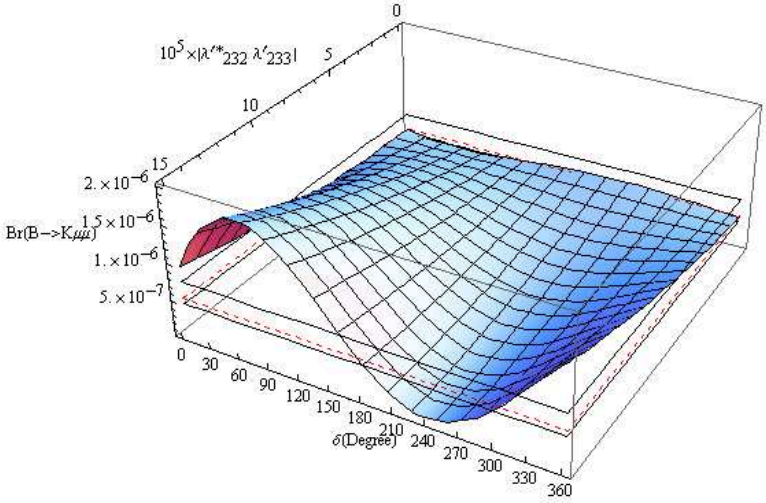

(d)

Fig 3. Dependence of total branching fraction with R-parity Yukawa coupling and its complex phase within 1σ (a, c) and 2 σ (b, d) level in observed value of branching fraction. The dashed plane represents the SM prediction of branching fraction. Single coupling dominance has been assumed. $\lambda'_{\alpha 33}\lambda'_{\alpha 32}$ (α=1, 2) is expressed in the units of $(\frac{m_{\tilde{u}_L}}{100\,GeV})^2$.

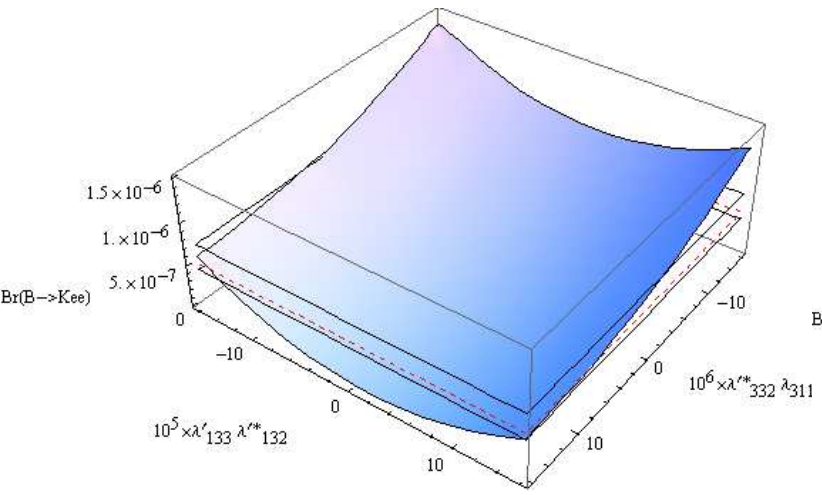

(a)

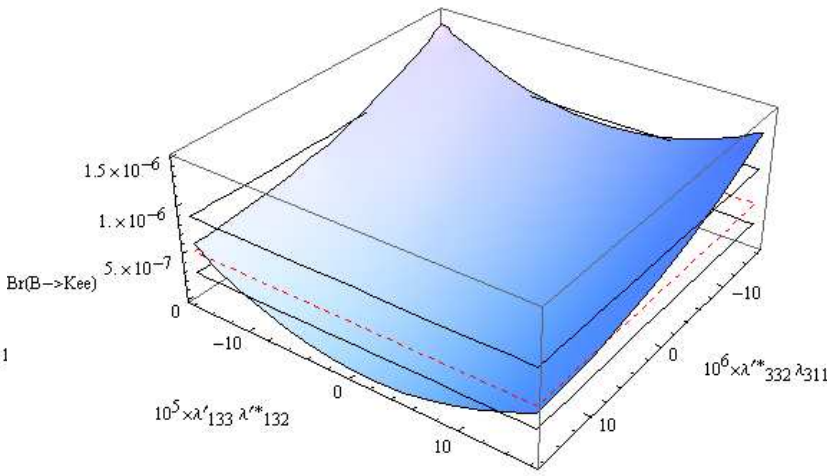

(b)

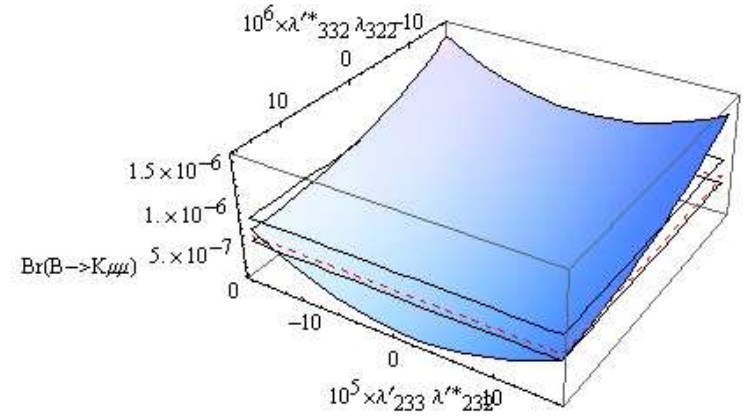

(c)

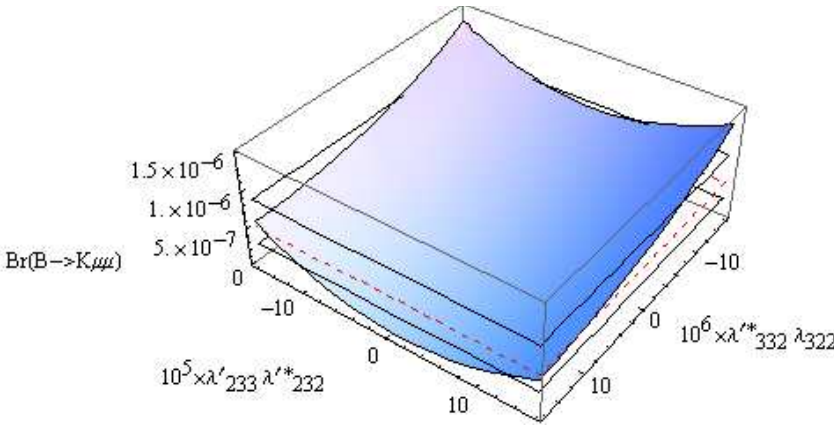

(d)

Fig 4. Dependence of total branching fraction with R-parity Yukawa coupling within 1σ (a, c) and 2 σ level (b-d) in observed value of branching fraction. The dashed plane represents the SM prediction of branching fraction. Single coupling dominance has been assumed. R-parity Yukawa couplings have been assumed real. $\lambda'_{\alpha 33}\lambda'_{\alpha 32}$ (α=1, 2) is expressed in the units of $(\frac{m_{\tilde{u}_{iL}}}{100\,GeV})^2$. $\lambda'_{332}\lambda_{3\alpha a}$ (α=1, 2) is expressed in the units of $(\frac{m_{\tilde{\nu}_L}}{100\,GeV})^2$.

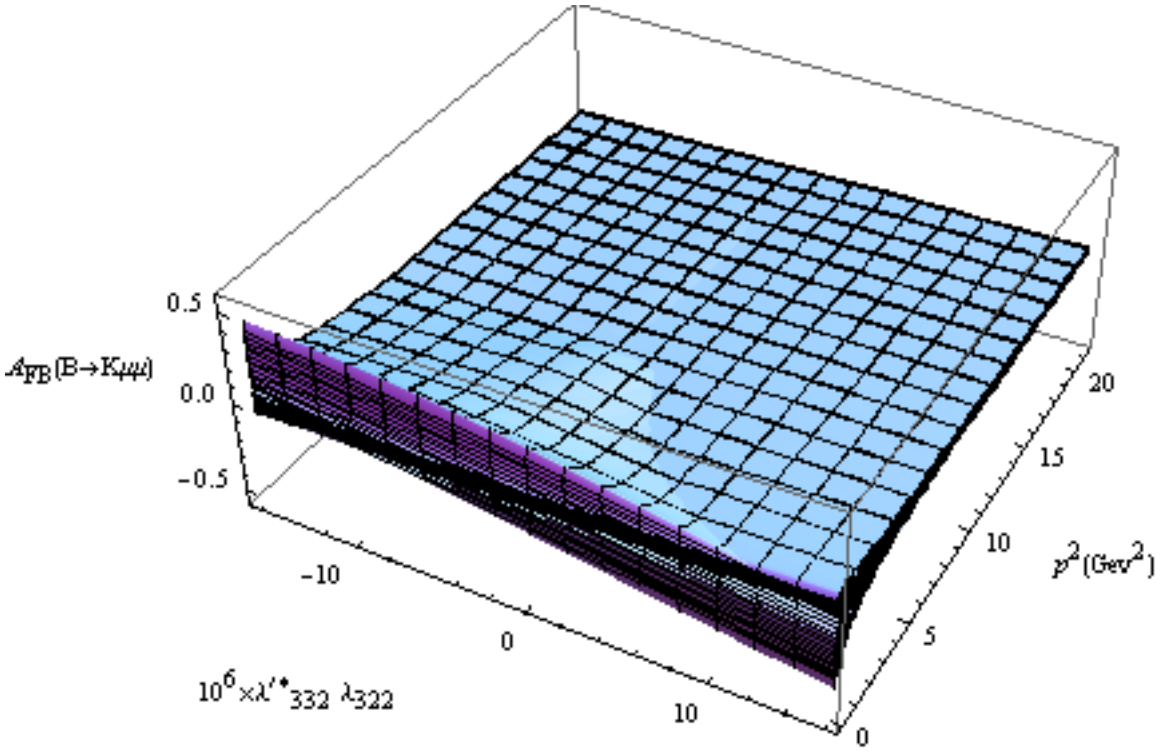

Figure 5: Variation of FBA w. r. t. Yukawa coupling $\lambda'_{332}\,\lambda_{322}$ and p^2 at various values of $\lambda'_{323}\,\lambda_{322}$ and $\lambda'_{233}\lambda'_{232}$ given by Ref [16]. $\lambda'_{332}\,\lambda_{322}$ is expressed in the units of $(\frac{m_{\tilde{\nu}_L}}{100\,GeV})^2$.

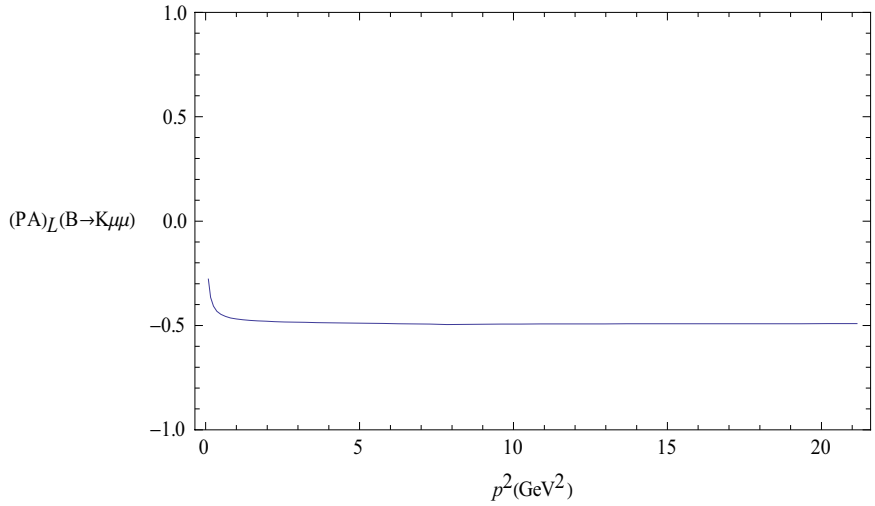

(a)

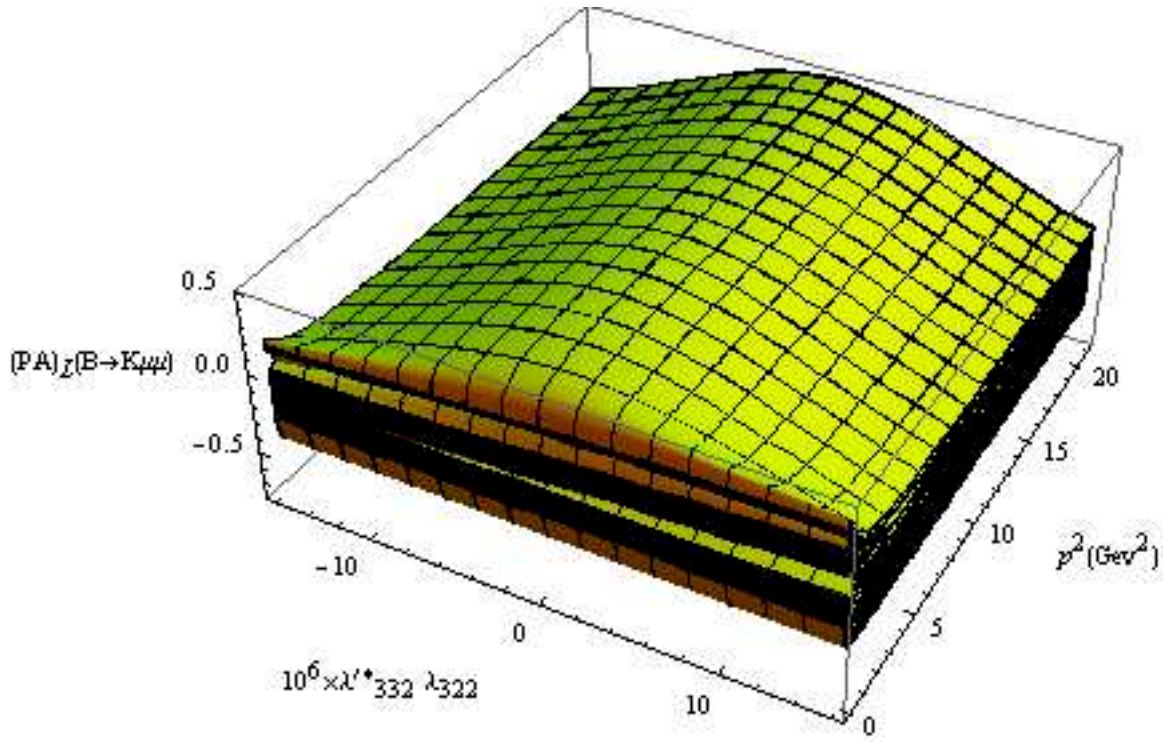

(b)

Figure 6: Variation of Longitudinal Polarization Asymmetry w.r.t. p^2 (a) in SM (b) and Yukawa $\lambda'_{332}\,\lambda_{322}$ at various values of $\lambda'_{323}\,\lambda_{322}$ and $\lambda'_{233}\lambda'_{232}$ given by Ref [16]. $\lambda'_{332}\,\lambda_{322}$ is expressed in the units of $(\frac{m_{\tilde{\nu}_L}}{100\,GeV})^2$.

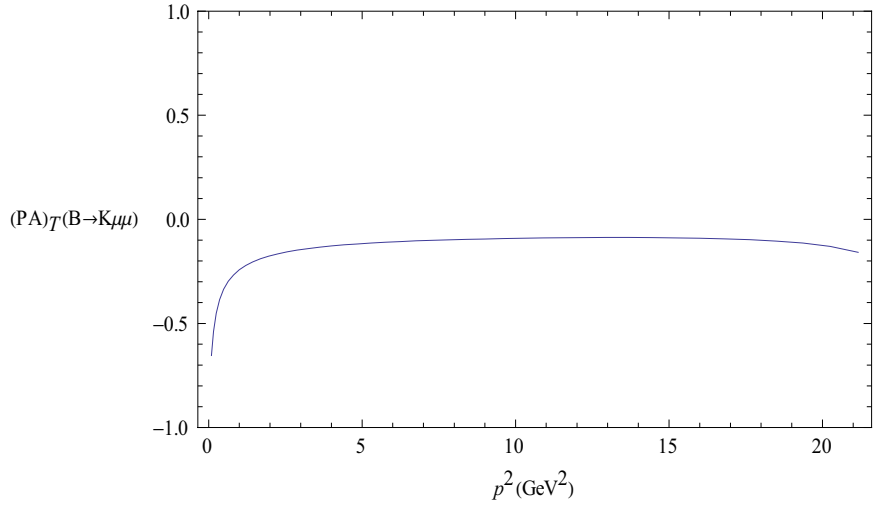

(a)

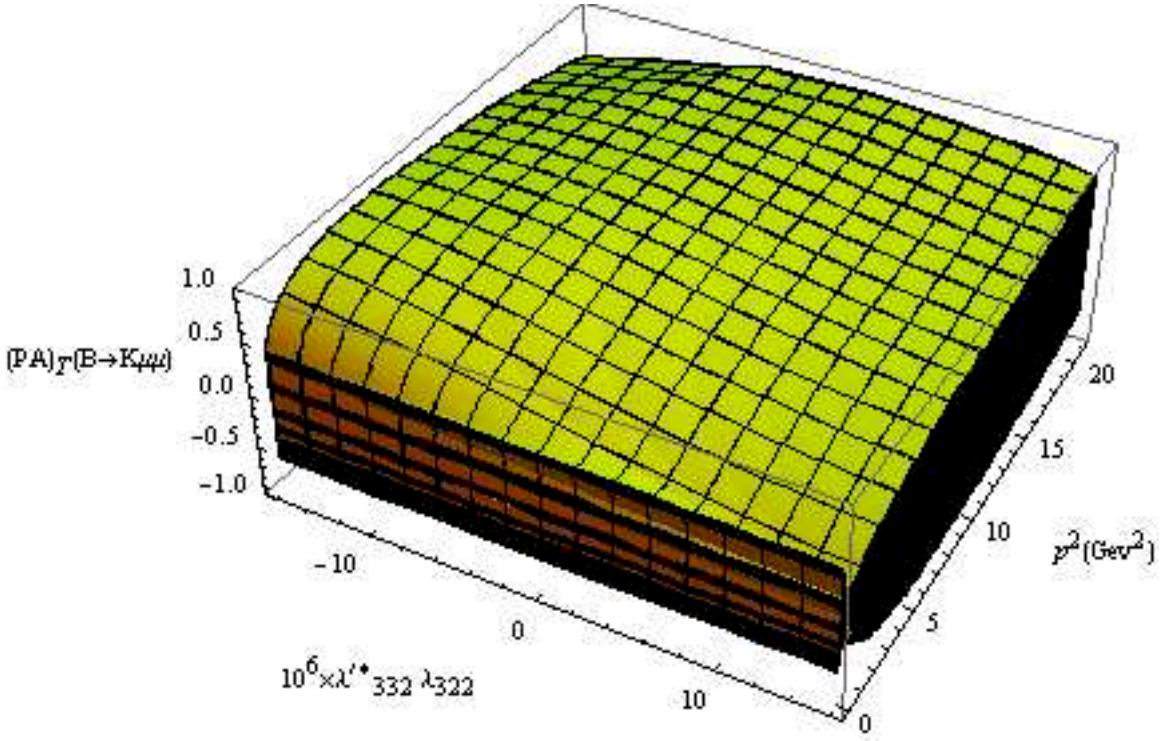

(b)

Figure 7: Variation of transverse polarization asymmetry w.r.t.p^2 (a) in SM (b) and $\lambda'_{332}\,\lambda_{322}$ at various values of $\lambda'_{323}\,\lambda_{322}$ and $\lambda'_{233}\lambda'_{232}$ given by Ref [16]. $\lambda'_{332}\,\lambda_{322}$ is expressed in the units of $(\frac{m_{\tilde{\nu}_L}}{100\,GeV})^2$.

<(PA)$_L$>(B−>Kμμ)

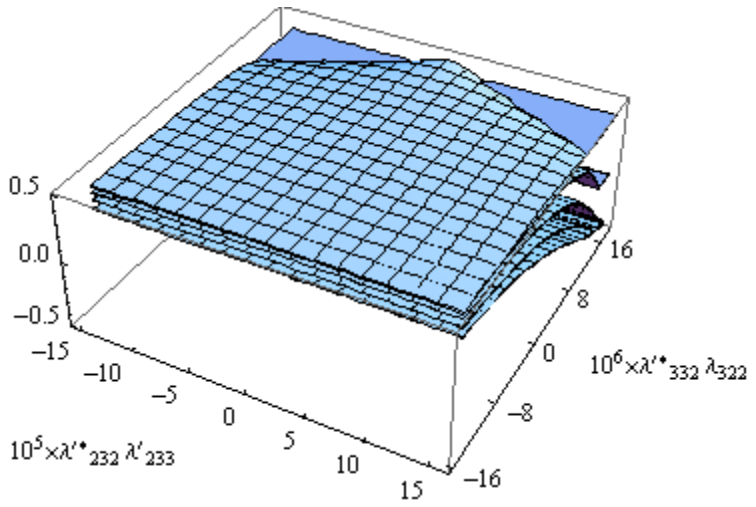

<(PA)$_L$>$_{SM}$=-0.49

(a)

<(PA)$_T$>(B−>Kμμ)

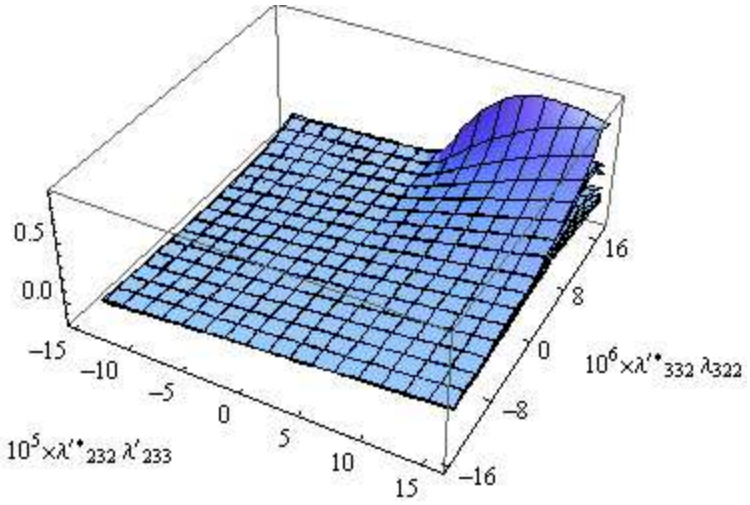

<(PA)$_T$>$_{SM}$=-0.11

(b)

Figure 8: Variation of (a) $<PA_L>$ (b) $<PA_T>$ w. r. t. $\lambda'_{332}\,\lambda_{322}$, $\lambda'_{233}\lambda'_{232}$ at various values of $\lambda'_{332}\,\lambda_{322}$, which are given by Ref [16]. $\lambda'_{332}\,\lambda_{322}$ is expressed in the units of $(\frac{m_{\tilde{\nu}_L}}{100\,GeV})^2$. $\lambda'_{232}\lambda'_{233}$ is expressed in the units of $(\frac{m_{\tilde{u}_L}}{100\,GeV})^2$.

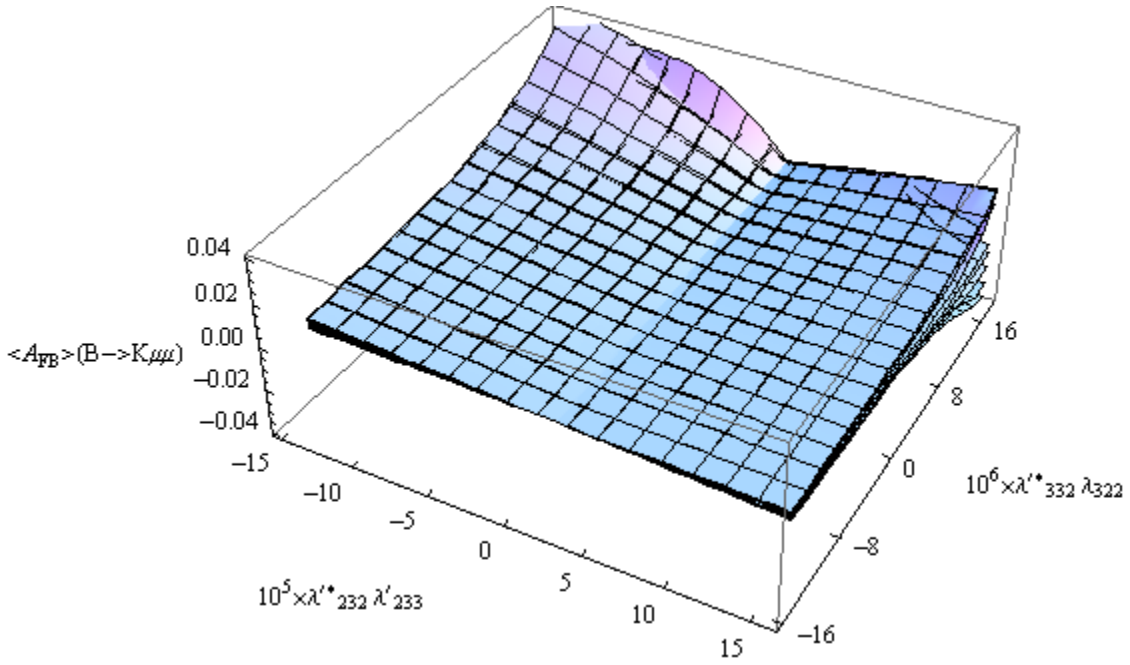

Figure 9: Variation of $<A_{FB}>$ w. r. t. $\lambda'_{332}\,\lambda_{322}$, $\lambda'_{233}\lambda'_{232}$ at various values of $\lambda'_{332}\,\lambda_{322}$, which are given by Ref [16]. $\lambda'_{332}\,\lambda_{322}$ is expressed in the units of $(\frac{m_{\tilde{\nu}_L}}{100\,GeV})^2$. $\lambda'_{232}\lambda'_{233}$ is expressed in the units of $(\frac{m_{\tilde{u}_L}}{100\,GeV})^2$.

<A_cp>=-0.001

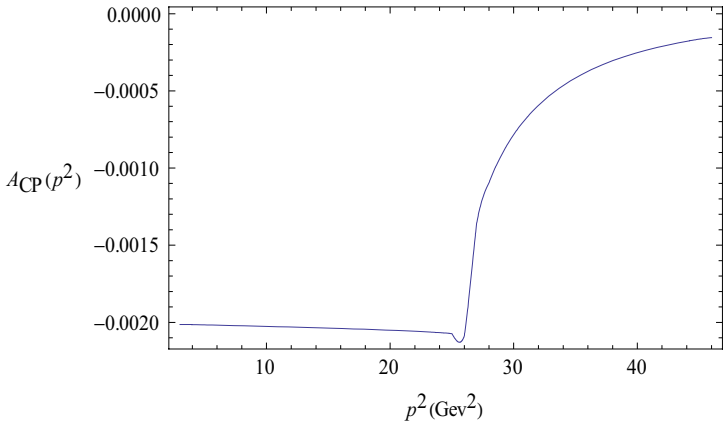

(a)

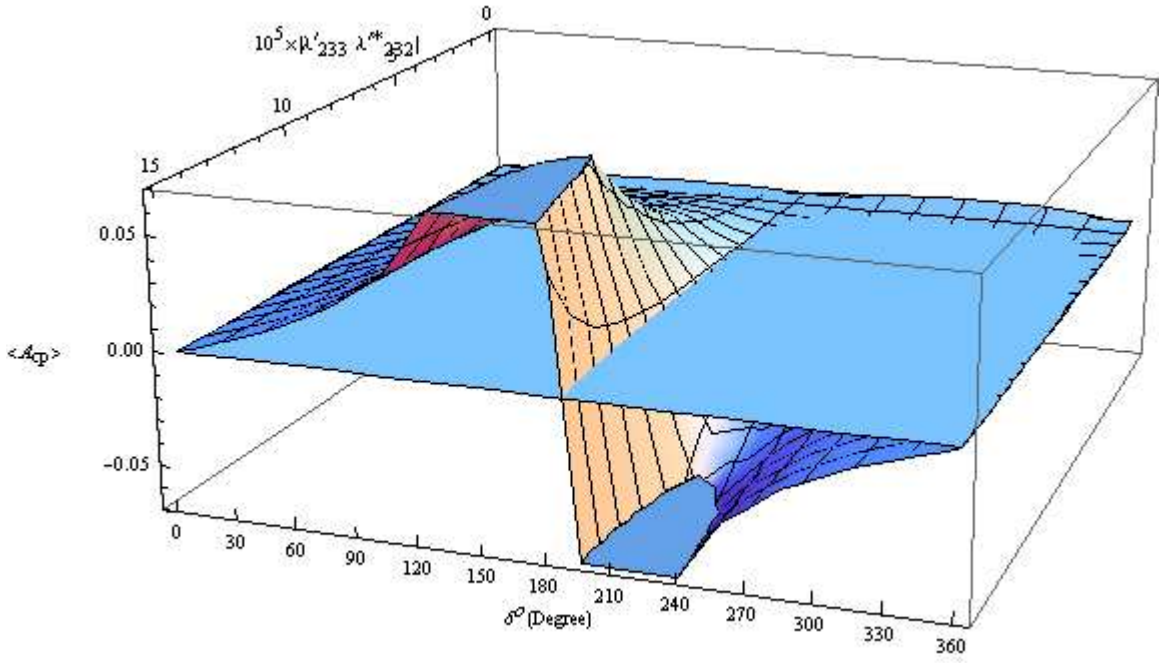

(b)

Figure10: (a) Plot showing variation of A_{cp} in SM. (b)Variation of <A_{CP}> w. r. t R-parity violating Yukawa coupling products. The shaded plane represents the SM prediction for A_{CP}. $\lambda'_{232}\lambda'_{233}$ is expressed in the units of $(\frac{m_{\tilde{u}_L}}{100\,GeV})^2$.